IIT KHARAGPUR RESEARCH MONOGRAPH SERIES

STRUCTURAL INTERMETALLICS and Intermetallic Matrix Composites

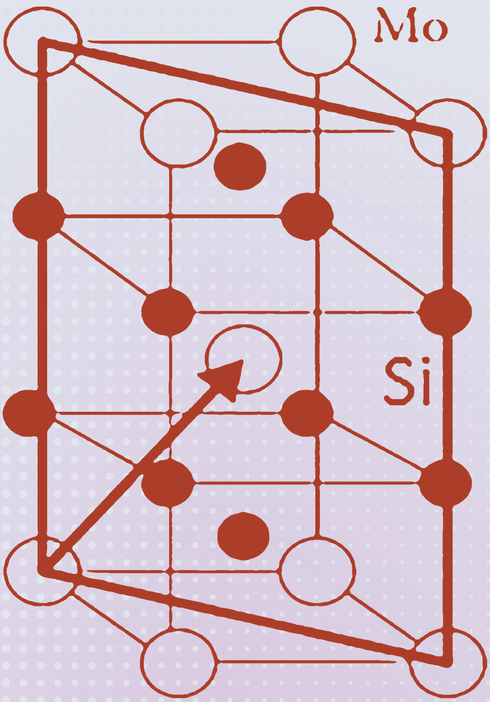

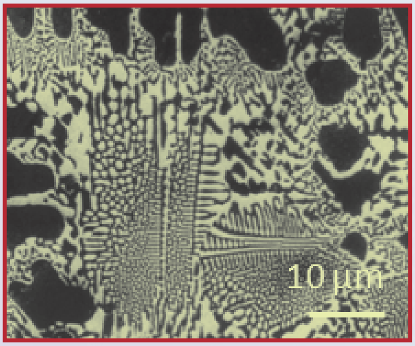

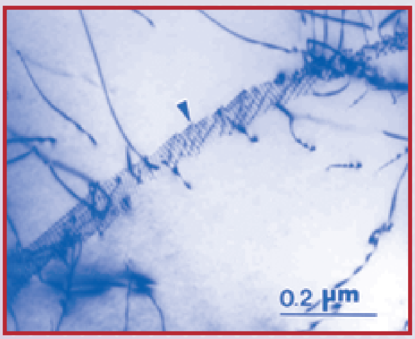

RAHUL MITRA

CRC Press
Taylor & Francis Group

STRUCTURAL INTERMETALLICS
and Intermetallic Matrix Composites

IIT Kharagpur Research Monograph Series

Published Titles:

Structural Intermetallics and Intermetallic Matrix Composites, *Rahul Mitra*

Digital Geometry in Image Processing, *Jayanta Mukhopadhyay, Partha Pratim Das, Samiran Chattopadhyay, Partha Bhowmick, and Biswa Nath Chatterji*

Mathematical Techniques for Wave Interaction with Flexible Structures, *Trilochan Sahoo*

Microfluidics and Microscale Transport Processes, *edited by Suman Chakraborty*

Modeling of Responsive Supply Chain, *M.K. Tiwari, B. Mahanty, S. P. Sarmah, and M. Jenamani*

Micellar Enhanced Ultrafiltration: Fundamentals & Applications, *Sirshendu De and Sourav Mondal*

STRUCTURAL INTERMETALLICS and Intermetallic Matrix Composites

RAHUL MITRA

CRC Press
Taylor & Francis Group
Boca Raton London New York

CRC Press is an imprint of the
Taylor & Francis Group, an **informa** business

CRC Press
Taylor & Francis Group
6000 Broken Sound Parkway NW, Suite 300
Boca Raton, FL 33487-2742

Version Date: 20150415

International Standard Book Number-13: 978-1-4665-1188-0 (eBook - PDF)

Visit the Taylor & Francis Web site at
http://www.taylorandfrancis.com

and the CRC Press Web site at
http://www.crcpress.com

Contents

List of Figures

Preface

Significant research has been carried out on structural intermetallics for several decades, involving both experimental and theoretical approaches. As a result, the structure–property relations of these materials are reasonably well understood, which has led to a road map for further research to develop high-performance materials for several diverse engineering applications. Work is in progress in many parts of the world to develop selected multicomponent intermetallic alloys based on silicides and aluminides for specific applications, particularly at elevated temperatures and in different types of extreme environments. Of course, there are excellent reviews and book chapters on many of these intermetallics. This monograph has been drafted as a part of the Diamond Jubilee Series of the Indian Institute of Technology Kharagpur. The author has been working on silicides for two decades and has also taught topics related to intermetallic alloys for a postgraduate course on advanced materials. A student learner often finds it difficult to grasp the complexities of the structure of intermetallics and their effect on various physical and mechanical properties. Keeping the requirement of students in mind, the first four chapters of this monograph are devoted to necessary fundamental aspects including thermodynamic principles, phase diagrams and crystal structures, processing methods, deformation and fracture mechanisms of ordered intermetallics, and oxidation behavior with mechanisms for protection against environmental degradation. The fifth chapter focuses on possible applications on the basis of the attractive properties of aluminides and silicides. The last four chapters contain exhaustive reviews of the existing literature on selected structural silicides and aluminides. The contents of this monograph are expected to be helpful to students interested in learning about intermetallics, as well as professionals beginning their research in this area.

The author would like to thank Professor K. K. Ray and Professor S. K. Roy, senior colleagues of his department, for their encouragement to write this monograph. The assistance received from Dr. Monali Ray, a postdoctoral fellow in my research group, in preparing the reference lists for different chapters in a very short time is gratefully acknowledged. The author owes a lot to all his students and collaborators for their contributions in extending my understanding of the subject. The author would also like to thank Dr. Gagandeep Singh and Ms. Marsha Pronin, editors at Taylor and Francis, for their valuable guidance during preparation of the manuscript. This monograph would not have been possible without the constant support and encouragement received from his wife, Mrs. Barnali Mitra, and daughter, Miss Rituparna Mitra, as well as the blessings of his parents, Mr. Paritosh Kumar Mitra and Mrs. Smrity Rani Mitra.

Rahul Mitra
Kharagpur, India

Abbreviations

APB	Antiphase boundary
APD	Antiphase domain
BDTT	Brittle-to-ductile transition temperature
CRSS	Critical resolved shear stress
CSF	Complex stacking fault
CSL	Coincidence site lattice
CT	Compact tension
CTE	Coefficient of thermal expansion
DS	Directionally solidified
EAM	Embedded atom method
HIP	Hot isostatically pressed
HP	Hot pressed
KW	Kear–Wilsdorf
LPPS	Low-pressure plasma spraying
MA	Mechanical alloying/mechanically alloyed
PM	Powder metallurgy
Poly	Polycrystalline
RT	Room temperature
SC	Single crystal
SEM	Scanning electron microscope
SENB	Single-edge notch bend
SHS	Self-propagating high-temperature synthesis
SISF	Superlattice intrinsic stacking fault
TEM	Transmission electron microscope
UHV	Ultrahigh vacuum
WB TEM	Weak-beam transmission electron microscopy

1

Phase Equilibria and Structure

1.1 Introduction

In many of the binary equilibrium phase diagrams for alloys, new phases are found at intermediate concentrations and their range of existence does not extend to pure components. Either these phases are line compounds or they are characterized by their nonstoichiometric composition and extended range of compositions. The line compounds with a fixed ratio of metallic components are often called *intermetallic compounds*. This terminology is appropriate only for stoichiometric compositions. It is not suitable for alloys with nonstoichiometric or extended range of compositions, and therefore such materials are referred to as intermetallic phases or alloys.

For substantial or complete solid solubility, the Hume-Rothery rules need to be satisfied: (i) the difference of atomic radii should not exceed 15%; (ii) the difference of electronegativity (chemical affinity) should be small; (iii) the crystal structures of solute and solvent must match; and (iv) the number of valence electrons should not be very different. The formation of intermetallic phases is preferred when the aforementioned rules are not satisfied. For example, both gold and copper have a face-centered cubic (fcc) structure, but the difference between their lattice constants is ≈12.8%, which promotes the formation of intermetallics in the Cu–Au system.

The formation and microstructural evolution of intermetallics depend on their thermodynamic stability. Very often, metastable phases with inhomogeneous compositions are formed through solidification, and suitable heat treatment is required for the evolution of equilibrium phases. For desirable mechanical properties or for carrying out forming operations, it may be necessary to stabilize desirable metastable phases through the addition of suitable alloying elements. Furthermore, the mechanical properties of the intermetallics are strongly dependent on their crystal structures. Hence, knowledge of phase equilibria along with crystal structures is necessary to understand the processing–structure–property relations of various binary and multicomponent intermetallic alloys.

1.2 Stability of Intermetallic Phases

A reduction of the Gibbs free energy of the system provides the driving force for the formation of intermetallics. The stability of the intermetallic phase depends not only on the reduction of free energy due to its formation but also on the free energies of the phases in equilibrium with the intermetallic phase. An example of a two-component system (A–B) is shown in Figure 1.1a.[1] In this system, α and β are solid-solution phases along with a stable intermetallic, I, and a metastable intermetallic, I′. In Figure 1.1b, the Gibbs free energies of the phases present at temperature T are plotted as a function of atomic fraction, $c = c_B$.[1] For the phases coexisting in equilibrium, the first derivatives of the Gibbs free energy (dG/dc) are equal, such that the chemical potentials or partial molal free energies are equal. Thus, common tangents can be drawn to G–c curves for the phases in equilibrium, as shown in Figure 1.1b. The stable intermetallic phase exists over the homogeneity range

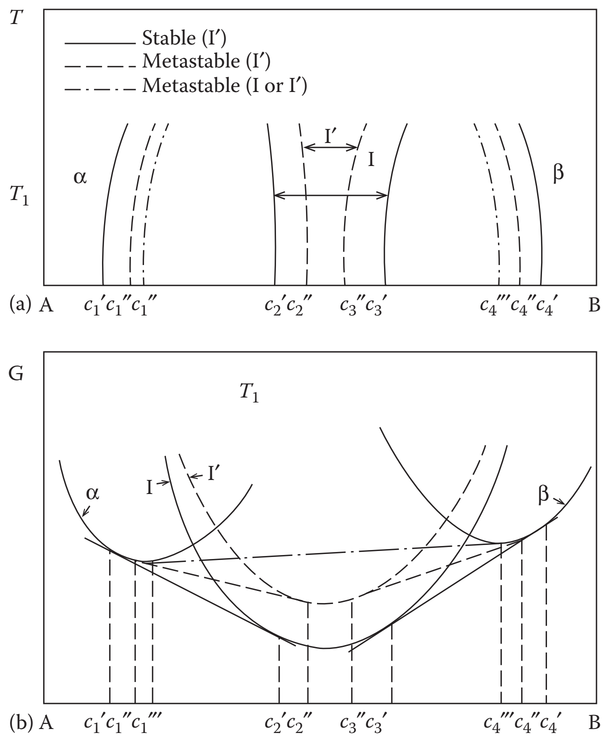

FIGURE 1.1
Schematic illustration of the thermodynamic stability of intermetallic phases (I = stable phase, I′ = metastable phase, α and β are solid-solution phases): (a) phase equilibria in the temperature (T)–composition (c) diagram; and (b) the corresponding free energy (G)–composition (c) diagram for true and metastable equilibria at absolute temperature, T_1.

between c_2' and c_3'. The atomic fractions of the phases α and β coexisting with I have compositions of c_1' and c_4', respectively. The metastable intermetallic phase, I′, exists over the narrower homogeneity range c_2'' to c_3''. The atomic fractions of the phases coexisting with I′ are the phases α and β, with compositions of c_1'' and c_4'', respectively.

The formation of ordered solid solutions is preferred in a binary alloy system if the bonding between unlike constituents is stronger than that between like atoms. In such cases, each atom tries to have the maximum number of unlike nearest neighbors. This is the example of a regular solution with large negative exchange energy[2]:

$$H_0 = H_{AB} - \frac{\left(H_{AA} + H_{BB}\right)}{2} \ll 0 \tag{1.1}$$

where H_{AB}, H_{AA}, and H_{BB} are the heats of formation of A–B, A–A, and B–B bonds, respectively. The heat of formation in the case of a binary intermetallic alloy system (such as Ni–Al or Fe–Al) varies with its composition, increasing to a maximum value and then decreasing. The variation of enthalpy with concentration for binary Ni-, Ti-, and Fe-aluminides is plotted in Figure 1.2 on the basis of the experimental data.[3–7] The heat of formation of intermetallics is usually determined using experiments based on solution calorimetry with the help of high-temperature calorimeters specially designed for such experiments.[8] First, the intermetallic alloy is dissolved in a liquid metal used

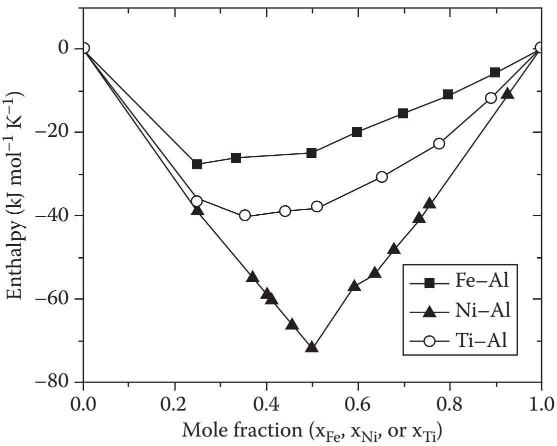

FIGURE 1.2
Plots depicting the variation of enthalpy of formation of binary intermetallic phases with temperature in Ni–Al, Ti–Al, and Fe–Al systems. The data have been taken from the literature. (From Desai, P. D., *J Phys. Chem. Ref. Data*, 16, 1, 109–124, 1987; Kubashewski, O. and W. A. Dench, *Acta Metall.*, 3, 339–346, 1955; Nash, P. and O. Kleppa, *J. Alloys Compd.*, 321, 228–231, 2001; Huang, W. and Y. A. Chang, *Intermetallics*, 6, 487–498, 1998; Samokhval, V. V., et al., *Russ. J. Phys. Chem.*, 145, 1174, 1971.)

as a solvent, and the heat of solution is determined. Subsequently, the heat of solution of the unreacted elemental mixture is measured. The difference between these two heats of solution provides the heat of formation of the intermetallic phase.

For stoichiometric intermetallic compositions, strictly periodic arrangements of atoms are attained. In the case of an intermetallic phase, AB, with the composition $c_A = 0.5$ and an ordered body-centered cubic (bcc) structure, the body-centered and corner positions of a unit cell are occupied by atoms of A and B, respectively, or vice versa. In other words, the ordered bcc unit cell comprises two simple cubic sublattices. If each sublattice site is occupied by only one type of atom, that is, either A or B, each A atom will have a B atom as its nearest neighbor.

1.3 Nomenclature of Crystal Structures

Two types of notation, Strukturbericht and Pearson's symbols, are normally used for the nomenclature of crystal structures of different intermetallic phases. Strukturbericht symbols are a partly systematic method for specifying the structure of a crystal. Here, the structures named A are monatomic (either X or Y, e.g., Al and Fe), Bs are diatomic with equal numbers of atoms of each type (XY, e.g., NaCl, NiAl, and FeAl), Cs have a 2:1 atomic ratio (X_2Y or XY_2, e.g., $MoSi_2$ and $NbSi_2$), D0s are 3:1 (XY_3 or X_3Y, e.g., Al_3Ti and Fe_3Al), E and H are used for perovskite and spinel structures, respectively, and Ls represent ordered cubic structures. It is customary to write the aformentioned structure notations with examples of real materials. A1 (fcc), A2 (bcc), A3 (hexagonal close-packed [hcp]), A4 (diamond), and A9 (graphite) are some examples of monatomic phases. The only example of A with a diatomic composition is the A15 structure, and the examples of intermetallic phases having this structure are Cr_3Si and Mo_3Si. Examples of diatomic phases are the B1 (NaCl), B2 (CsCl), B3 (zinc blende), and B11 (CuTi) structures. Similarly, typical C-type structures are $C11_b$ ($MoSi_2$), C14 (Laves—$MgZn_2$), C49 ($ZrSi_2$), etc., whereas typical D-type structures are $D0_{11}$ (Fe_3C, cementite), $D0_{22}$ (Al_3Ti), $D0_{23}$ (Al_3Zr), etc. Some of the L-type structures are $L1_0$ (AuCu), $L1_1$ (CuPt), $L1_2$ (Cu_3Au), etc.

The crystal structures of the intermetallics can be any of the seven Bravais lattices: cubic (c), hexagonal and rhombohedral (h), tetragonal (t), orthorhombic (o), monoclinic (m), and triclinic (a). The unit cells with each of these crystal structures can further be classified as primitive (P), body centered (I), face centered (F), side-face centered or base centered (S), and rhombohedral (R). Fourteen possible Bravais lattices are represented by the following notations: primitive cubic (cP), face-centered cubic (cF), body-centered cubic (cI), rhombohedral hexagonal (hR), primitive hexagonal (hP), primitive tetragonal (tP), body-centered tetragonal (tI), primitive orthorhombic (oP), body-centered orthorhombic (oI), face-centered orthorhombic (oF), side-centered orthorhombic (oS), primitive monoclinic (mP), side-centered monoclinic (mS), and primitive triclinic (aP). Besides the nature of the atomic arrangement, the number of atoms per unit cell is also included in the notation for a complete description of the unit cell. For example, the notation for the structure of any ordered fcc alloy can be written as cP4, as there are four atoms in its unit cell. In a similar manner, a body-centered, tetragonal-structured unit cell with eight atoms can be referred to as tI8.

1.4 Crystal Structures and Phase Diagrams of Silicides

The major silicide phases of interest for high-temperature structural applications are drawn from the following binary phase equilibrium systems: Mo–Si, W–Si, Ti–Si, Nb–Si, and Cr–Si. The crystal structures and lattice constants of different silicide-based intermetallics are shown in Table 1.1.

1.4.1 Molybdenum Silicides

The binary Mo–Si phase diagram shows the presence of stoichiometric compounds with compositions Mo_3Si and $MoSi_2$.[9] On the other hand, Mo_5Si_3 has a homogeneity range of 3 at.% Si. While $MoSi_2$ has a body-centered tetragonal (bct) structure ($C11_b$, tI8) with eight atoms in the unit cell (Figure 1.3a), the tetragonal unit cell of Mo_5Si_3 has 32 atoms (20 Mo atoms and 12 atoms of Si, $D8_m$, tI32) (Figure 1.3b).[10] Mo_3Si has a cubic structure (A15, cP8) comprising eight atoms in its unit cell, with six atoms of Mo and eight atoms of Si (Figure 1.3c). The bct structure of $MoSi_2$ has a fixed *c*/*a* ratio of 2.452 and appears similar to three bcc unit cells, stacked one on top of another with the body-centered site occupied by the atom of Mo or Si, alternately. It has been shown by Francwicz[11] that the *c*/*a* ratio of approximately 2.45 remains unchanged with minor alloying of tetragonal-structured $MoSi_2$, and is essential for the stability of $C11_b$ crystal structure. Alloying with transition-metal elements such as Nb, Ti, and Cr, having an atomic radius and an electronic structure close to those of Mo, substitutes Mo sites, while alloying elements such as Al with atomic radius comparable to Si occupy the Si sublattice sites. Alloying $MoSi_2$ with other elements to an extent that exceeds the limit of 3 at.% has been observed to affect the stability of the bct structure.

$MoSi_2$ has a hexagonal structure (C40, hP9) (Figure 1.3d) at high temperature (1900°C). The lattice vectors of $Mo(Si,Al)_2$ formed on alloying with Al in excess of 3 at.% also possess C40 structure.[12–14] Interestingly, the *c*/*a* ratio for the perfect hexagonal arrangement is $6^{1/2} = 0.2449$ nm,[15] which is very close to that of the $C11_b$ structure ($c/a = 0.2452$ nm). The [001], ½[111], ½[331], and [110] directions in the $C11_b$ (110) plane are equivalent to $[01\bar{1}0]$, $1/3[11\bar{2}0]$, $[01\bar{1}0]$,

TABLE 1.1

Crystal Structure and Lattice Constants of Silicides

Silicides	Crystal Structure	Structure and Space Group	Lattice Parameters (nm)
$MoSi_2$	Body-centered tetragonal	$C11_b$ (tI6), I4/mmm	$a=0.3202$ $c=0.7845$
Mo_5Si_3	Body-centered tetragonal	$D8_m$ (tI32), I4/mcm	$a=0.959$ $c=0.487$
Mo_3Si	Cubic	A15 (cP8) Pm3n	$a=0.4892$
Mo_5SiB_2	Body-centered tetragonal	$D8_1$ (tI32), I4/mcm	$a=0.6013$ $c=1.103$
$Mo(Si,Al)_2$	Hexagonal	C40 (hP9), $P6_222$	$a=4.644$ $c=6.548$
WSi_2	Body-centered tetragonal	$C11_b$ (tI6), I4/mmm	$a=0.3211$ $c=0.7868$
Ti_5Si_3	Hexagonal	$D8_8$ (hP16), I4/mcm	$a=0.7444$ $c=0.5143$
$NbSi_2$	Hexagonal	C40 (hP9) $P6_222$	$a=4.7971$ $c=6.592$
Nb_5Si_3	Body-centered tetragonal	α: $D8_1$ (tI32) β: $D8_m$ I4/mcm	α phase: $a=0.656$ $b=1.187$ β phase: $a=1.0$ $b=0.507$
$CrSi_2$	Hexagonal	C40 (hP9) $P6_222$	$a=0.4428$ $c=0.6363$

Source: Mitra, R., *Inter. Mater. Rev.* 51, 1, 13–64, 2006.

and $1/3[\bar{2}110]$, respectively, in the C40 (0001) plane. While the $C11_b$ structure is characterized by ABAB… type stacking along the *c* axis, the C40 lattice shows ABCABC… type stacking. Hence, a stacking fault in the (110) plane of the $C11_b$ lattice would lead to the creation of localized C40-type structure.

The tetragonal structure of Mo_5Si_3 is quite different from that of $MoSi_2$ (compare Figure 1.3a and b), as the former material exhibits the following characteristics:[16] (i) the value of a (lattice parameter) is greater than c such that $a/c \approx 2$; (ii) close-packed planes are absent; and (iii) the –Si–Mo–Si– chains are along the [100] and [010] directions, while the –Mo–Mo– and –Si–Si– chains are along the [001] direction. In $MoSi_2$, the close-packed planes and directions are distinct, and the –Si–Mo–Si– chains in $MoSi_2$ are along the [001] direction, while the –Mo–Mo and –Si–Si chains are along the [100] and [010] directions. The interatomic bond along the [001] direction containing the –Si–Mo–Si– chain is believed to be stronger and more directional compared with either Mo–Mo or Si–Si bonds.

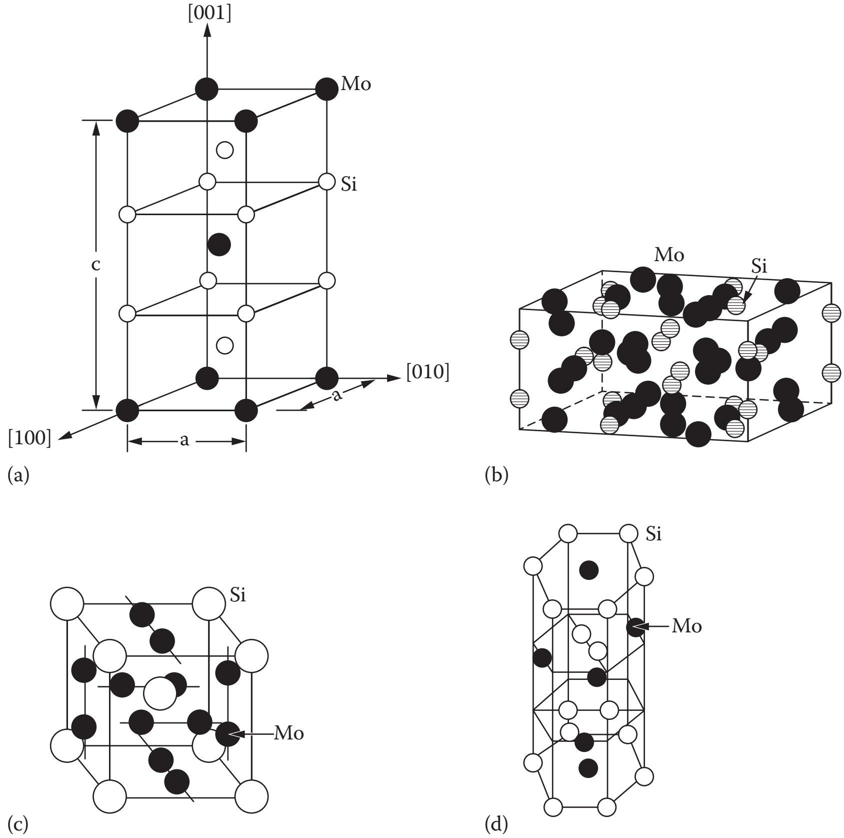

FIGURE 1.3
Schematic illustrations depicting the unit cells of (a) $MoSi_2$ ($C11_b$, tP8); (b) Mo_5Si_3 ($D8_m$, tI32); (c) Mo_3Si (A15, cP8); and (d) $MoSi_2$ (C40, hP9).

The Mo-rich section of the ternary isothermal phase diagram[13] of the Mo–Si–B system corresponding to 1600°C is shown in Figure 1.4. Mo–Si–B ternary alloys can be designed to have the optimum volume fractions of α-Mo, Mo_3Si, and Mo_5SiB_2 phases. All three phases have a nearly fixed composition with a limited solubility for other elements and hence provide microstructural stability at high temperatures. The α-Mo phase has a bcc structure with the solubility for Si and B atoms being 3 and <1 at.%, respectively, while the Mo_3Si possesses a single-phase composition close to 76Mo–24Si (at.%).[17] On the other hand, Mo_5SiB_2 possesses a bct structure ($D8_1$, tI32) with 32 atoms in the unit cell, comprising 20 atoms of Mo, 4 atoms of Si, and 8 atoms of B (Figure 1.5). In the unit cell of Mo_5SiB_2, three layers can be identified, the first comprising only Mo atoms, the second having only Si atoms, and the third having a mixture of Mo and Si atoms. It is interesting to note that the Mo-nearest neighbors

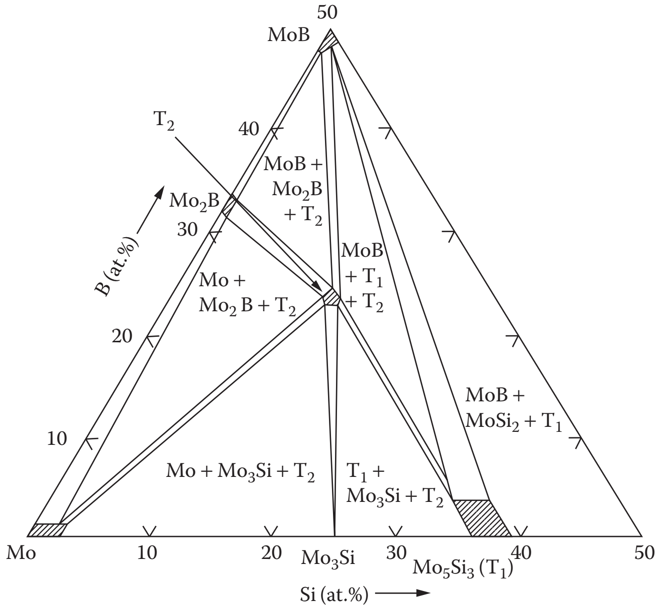

FIGURE 1.4
The Mo-rich section of the ternary isothermal phase diagram of the Mo–Si–B system corresponding to 1600°C. The position of Mo_5SiB_2 in this phase diagram is shown as T_2.

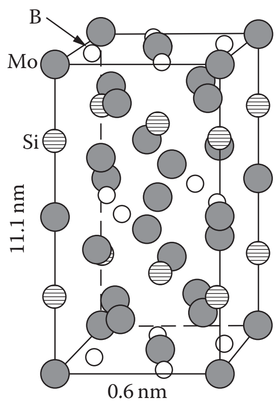

FIGURE 1.5
Schematic illustration of the unit cell of Mo_5SiB_2 ($D8_1$, tI32).

of the Mo sites in the unit cell are in bcc arrangement, which implies that the solubility of transition-metal atoms in Mo_5SiB_2 is similar to that in the bcc-Mo. The coefficient of thermal expansion anisotropy (α_c/α_a) of Mo_5SiB_2 has been found to be 1.4 at 500°C,[18] which is significantly lower than that (≈2.2) of Mo_5Si_3.[16]